

Energy Harvesting and Mission Effectiveness for Small Unmanned Aircraft

Mark J. Cutler* Timothy W. McLain†
Randal W. Beard‡

Brigham Young University, Provo, Utah, 84602 USA

Brian Capozzi§
Mosaic ATM, Leesburg, Virginia, 20175 USA

This paper explores the feasibility of improving unmanned air vehicle (UAV) mission effectiveness by extracting energy from the atmosphere. Specifically, we consider an aerial surveillance mission in the vicinity of a geographic ridge. Cross winds flowing over the ridge produce regions of lift on the windward side that can be exploited to increase mission duration. Mission effectiveness is quantified using the seeability metric. Simulation results are presented for several observation target placements. Results indicate that seeability and imaging persistence can be improved by exploiting ridge lift. Simulations demonstrated that targets at ranges less than four times the ridge height were able to be observed over an indefinite period by a UAV with a glide ratio of 11:1.

I. Introduction

For small unmanned air vehicles (UAVs) atmospheric effects, such as vertical wind components, thermals, gusts, and wind gradients, represent significant sources of energy that an aircraft can potentially tap to increase endurance and range. These effects are typically transient and geographically dependent, thus the ability to exploit them as an energy resource requires the ability to detect them and characterize their size and location. For intelligence, surveillance, and reconnaissance (ISR) missions, the objective is often to provide persistent observation of a target of interest. The goal of this paper is to explore the effectiveness of energy harvesting and its potential to enhance ISR mission effectiveness. The primary challenge associated with harvesting atmospheric energy and performing ISR simultaneously is that they are competing objectives likely requiring the UAV to perform in characteristically different ways to be successful. Furthermore, the time and location of atmospheric energy sources may not coincide with the time and location of the target of interest.

As an example scenario, we have chosen to investigate the observation of a target in close proximity to a ridge with prevailing winds blowing over the ridge providing upward vertical wind components along the windward edge of the ridge as shown in Figure 1. This is typical of what might be encountered in a mountain valley or along a coastal dune or bluff. We will first consider a scenario with the target and vertical wind source in close proximity and then explore scenarios with the target and energy source at increasing separation distances.

As a measure of mission effectiveness, we propose to use the notion of seeability first introduced by Morse et al.¹ The seeability metric was developed for wilderness search and rescue missions utilizing small unmanned aircraft to assist in the search. Early field trials showed that high quality video imagery was critical to the success of the search mission. The seeability metric was formulated as means of quantifying video image quality. Initially the metric focused on the viewing range and angle, but was later modified to include viewing angle uniqueness and lighting conditions.^{1,2}

*Research Assistant, Mechanical Engineering, markjcutler@gmail.com, AIAA Member.

†Professor, Mechanical Engineering, mclain@byu.edu, AIAA Associate Fellow.

‡Professor, Electrical and Computer Engineering, beard@byu.edu, AIAA Associate Fellow.

§Principal Analyst, bcapozzi@mosaicatm.com, AIAA Member.

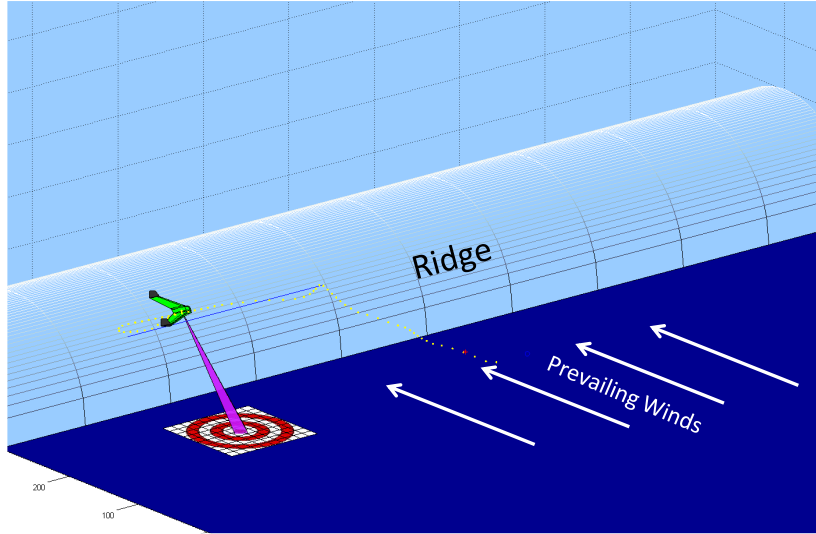


Figure 1. Energy harvesting ISR scenario.

Atmospheric energy harvesting for increased range and endurance is not a new concept. Birds have been observed flying hundreds of kilometers without flapping their wings by taking advantage of thermal and ridge lift. Manned sailplane and hang glider pilots also routinely use energy available in the air for long-distance, long-duration cross-country flight. Autonomous atmospheric energy harvesting for small UAVs has become an active area of research in recent years. Wharington³ first suggested autonomous soaring, or the use of thermals, in 1998 to increase small UAV endurance. Allen^{4,5} and Edwards⁶ recently demonstrated flight results of autonomous thermal soaring algorithms. Langelaan⁷ explored optimal flight trajectories for minimum flight time and maximum energy gain while traversing a ridge. Exploiting ridge lift for stationary target observation has not yet been explored. The goal of this work is to investigate the potential for energy harvesting to enhance the effectiveness of an ISR mission.

II. Technical Approach

This section describes the technical approach taken in investigating ISR mission effectiveness while harvesting energy from vertical wind components near a ridge line. Section A describes the seeability metric used as a measure of mission effectiveness, while Section B describes the wind model used for flow over a ridge and the algorithm utilized to harvest energy from the vertical components of the wind near the ridge.

A. Seeability Metric

The concept of seeability was first developed in response to needs observed during wilderness search and rescue (WiSAR) field training exercises. In these experiments, small UAVs were used to perform aerial searches for lost individuals. A key observation from early experiments was that search victims were often difficult to detect, even when the UAV sensor footprint passed over them repeatedly. The need to quantify the quality of video imagery was clearly evident. The seeability metric was developed to fill this need.

Morse, et al.¹ defined the seeability metric for a point i in camera frame j as

$$S_{ij} = \begin{cases} \frac{\mathbf{n}_i \cdot \mathbf{v}_{ij}}{1+d_{ij}/\alpha} & \text{if point } i \text{ is visible in frame } j, \\ 0 & \text{otherwise,} \end{cases} \quad (1)$$

where \mathbf{n}_i is the terrain surface normal, \mathbf{v}_{ij} is the pointing direction of the camera, d_{ij} is the distance from the camera to point i , and α is a scaling factor. This represents the instantaneous seeability, which is a measure of how well a particular point on the ground can be seen at a particular instant of time. The notion of cumulative seeability was also defined, which captures the cumulative benefit of multiple unique views of

the point of interest. The seeability concept has been extended by Niedfeldt et al.² to include target size, target/background contrast, and lighting/shading.

The instantaneous seeability metric specified in (1) was modified slightly for use in this study and is given by

$$S = \frac{\cos(\phi - \phi^*)}{1 + (D/d)^2} \quad (2)$$

where ϕ is the viewing angle (measured from vertical), ϕ^* is the optimal viewing angle, d is a normalizing quantity for distance, and D is the distance or range from the camera to the target. In this paper, we assume that the optimal viewing direction is directly above the target, i.e., $\phi^* = 0$. For scaling, a value of $d = 300$ m was used. Seeability versus target distance and viewing angle is plotted in Figure 2. As expected, seeability is high when the UAV is over the target and within a specified altitude.

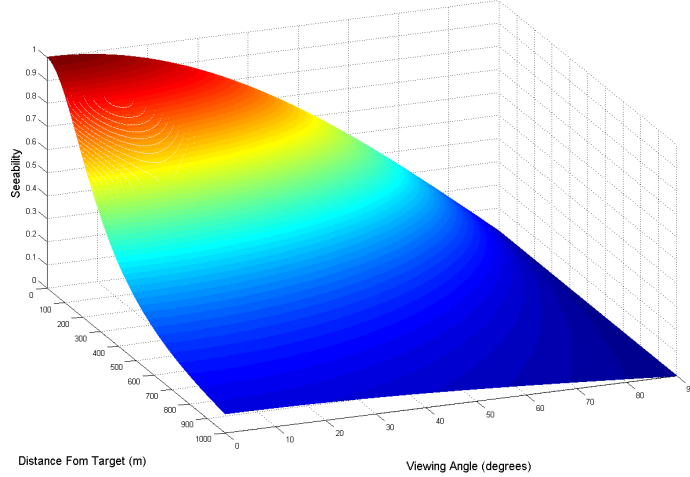


Figure 2. Seeability as a function of distance from target and viewing angle

In this work, our primary objective is to maintain persistent observation of a target while keeping seeability above a desired threshold. Time over target is of prime importance. Our metric for mission effectiveness will be the time that seeability is maintained above a specified level of 0.5 during the mission.

B. Ridge Soaring

In the simulation studies presented, we modeled orographic lift using an idealized cylindrical ridge similar to that presented by Langelaan.⁷ The ridge was oriented north-south with a constant velocity wind blowing from west to east. The vertical wind velocity gradient due to wind shear was modeled as

$$w_\infty = w_6 \frac{\ln(h/z_0)}{\ln(6/z_0)} \quad (3)$$

where w_6 is the wind speed at 6 m above ground level and z_0 is defined as 0.65 m.⁸ For the current simulation w_6 is 4 m/s (about 1/3 the nominal airspeed on the simulated UAV). The gradient profile is shown in Figure 3.

The horizontal and vertical components of the wind field as it flows over a half-cylinder ridge of radius R are given by

$$w_e = w_\infty + w_\infty \frac{R^2}{r^2} (\sin^2 \theta - \cos^2 \theta) \quad (4)$$

$$w_d = -2w_\infty \frac{R^2}{r^2} \sin \theta \cos \theta \quad (5)$$

where w_e and w_d are the wind magnitudes in the east and down directions respectively. As shown in Figure 4, the position of the UAV relative to the ridge is defined by the distance r and the angle θ . Streamlines over

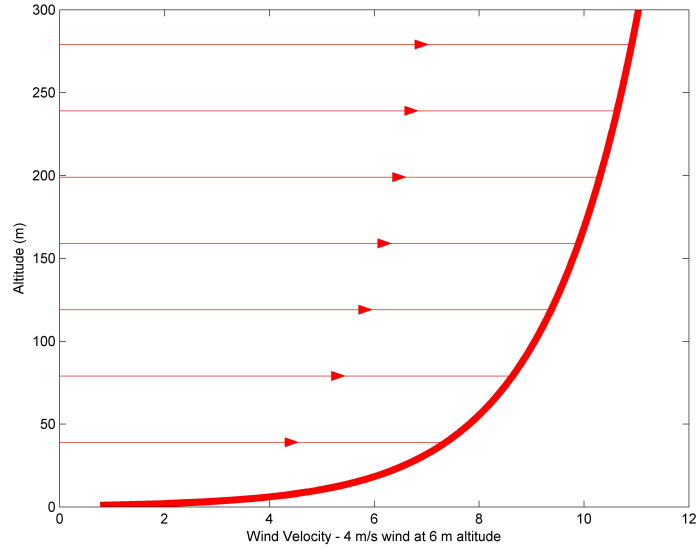


Figure 3. Vertical velocity gradient as a function of altitude

the half-cylinder ridge model are shown in Figure 5 as well as the region where ridge lift can be utilized to harvest energy in the form of altitude by flying back and forth parallel with the ridge in a sweeping pattern, always turning upwind.

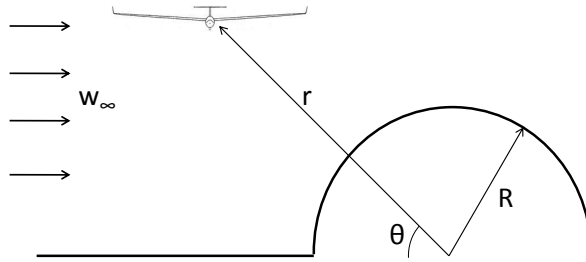


Figure 4. Soaring along a cylindrical ridge

Solving Equation (5) for maximum lift (minimum w_d) shows that the best lift occurs along the line $\theta = \pi/3$. Along this line, the vertical component of the wind is proportional to the inverse of the square of the distance from the ridge

$$w_d|_{\theta=\pi/3} = -\frac{\sqrt{3}}{2} w_\infty \frac{R^2}{r^2}. \quad (6)$$

As r becomes large relative to R , w_d approaches zero, indicating that potential altitude gain from a ridge is

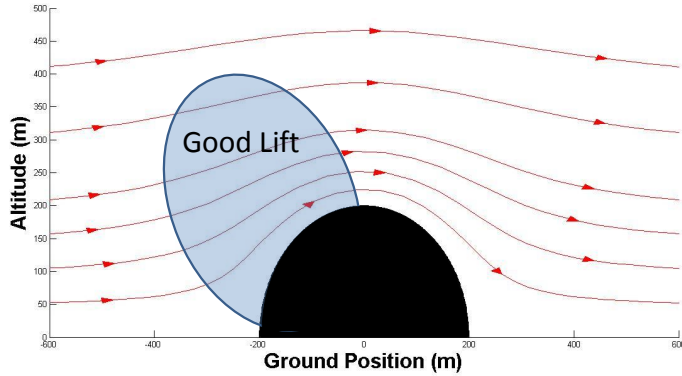


Figure 5. Streamlines over an ideal cylinder

constrained by ridge size and wind velocity.

The optimal ridge soaring trajectories explored by Langelaan⁷ assumed that the UAV flew in the 2 dimensional plane defined by $\theta = \pi/4$, and that UAV altitude never dropped below the maximum height of the ridge. The research presented here builds upon Langelaan's work by modeling the UAV flight in three dimensions and investigating the performance of the UAV as it deviates from ideal lift zone or drops below the height of the ridge.

III. Simulation Environment

Simulations of a UAV harvesting atmospheric energy while simultaneously maintaining ISR mission effectiveness were conducted in a modified version of BYU's Aviones simulation environment. Aviones is a twelve-state six-DOF UAV simulator built within Matlab-Simulink. The simulated aircraft is a battery-powered one-meter flying wing. The nominal airspeed of the UAV was 11 m/s, while its glide ratio was 10.9:1. Aviones is capable of simulating complex aerodynamic effects of flight through different wind environments (e.g., thermals, ridge lift, velocity gradients, etc.). To explore ISR mission effectiveness while harvesting energy, a mountain valley was simulated with a 1 km by 1 km flat valley floor and a 100 m half cylinder ridge along the eastern edge as shown in Figure 6. The wind was blowing towards the east at 4 m/s at an altitude of 6 m (see Figure 3) so that useful lift was found on the western edge of the ridge. Three different target locations, located 100, 400, and 700 m west of the ridge, were used. The UAV was controlled to fly from the starting location to the target of interest. From there, the UAV sought to harvest energy from the ridge while observing the target. Waypoints over the target and along the ridge were used to guide the UAV. The UAV followed the waypoint paths using a vector-field path following algorithm.^{9,10}

Current target observation algorithms typically consist of flying to the target location and maintaining altitude in an overhead circling pattern until battery power reaches a low-level threshold. This target observation technique is commonly used regardless of wind conditions, with the path following controller fighting any deviation caused by wind. Although circling over a target may be sufficient in certain cases, this strategy is inevitably limited by the available battery power. If, as in the case of persistent surveillance, increasing time over target is a primary objective, target observation strategies that allow for energy harvesting can be employed in certain cases to increase flight time while maintaining adequate seeability.

For the energy harvesting ISR missions simulated in this work involving a UAV near a ridge, the following sequence of mission phases for increasing time over target was followed:

1. Transition from starting location to target.
2. Fly to ridge base.
3. Gain altitude until the upper altitude threshold is met.
4. Fly to target.
5. Circle over target until the lower altitude threshold is met.

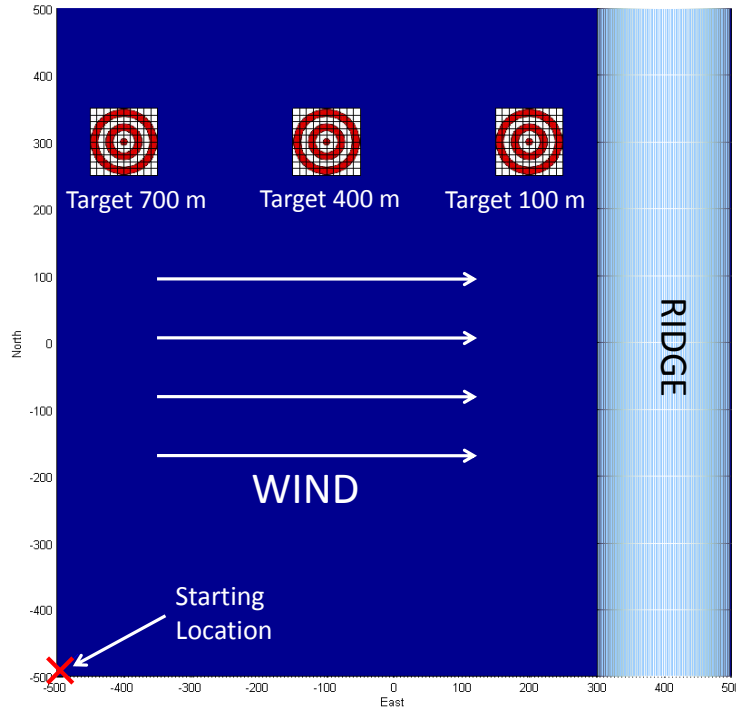


Figure 6. Aviones simulation environment

If the target is close enough to the ridge so that the viewing angle yields acceptable levels of seeability, phases 1, 2, and 3 are followed while observing the target. If the target is too far away to feasibly observe the target, phases 1 through 5 will be followed with phases 2 through 5 being repeated until the mission is complete or UAV battery energy is depleted.

In the Aviones environment, each simulation run starts from the southwest corner of the flying field at ground level. Phase 1 consists of flying under battery power towards the target, climbing to the lower altitude threshold level of 50 m. Once the target has been observed, the UAV continues to the base of the ridge under its own power as specified in phase 2. Phase 3 is the energy harvesting phase. Starting with 50 m of altitude, the UAV shuts off its motor and begins soaring along the ridge in a 200 m long sweeping pattern. The UAV gains energy in the form of altitude by taking advantage of the upward component of wind created by the airflow over the ridge. If the UAV is able, it is commanded to fly along the line of greatest lift as specified in Equation 6. While the UAV altitude is below the top of the ridge (100 m), it is commanded to fly along the profile of the ridge with a 45 m safety factor. The commanded east position of the UAV as a function of altitude is plotted in Figure 7.

Once the UAV has reached the upper altitude threshold of 175 m it turns west and begins an unpowered glide towards the target during phase 4. When the UAV is over the target (phase 5) it begins a circling descent, observing the target until the lower altitude threshold is met. If, as in the case of target 2 below, enough altitude remains after observing the target, the UAV will return to the base of the ridge without expending its own power; however, if in any case the UAV altitude drops below 50 m, the motor automatically turns on to keep the UAV at a safe altitude.

IV. Results and Discussion

Each of the three target locations shown in Figure 6 was observed using the two different observation techniques discussed above, 1) the traditional method of tracking an orbit by fighting the wind to maintain altitude and position on the orbit, and 2) using an energy harvesting approach to improve time over target while maintaining seeability. During each simulation the following data were collected and are displayed with each simulation result below: instantaneous seeability, battery energy consumed, battery power expended, and flight altitude. Each simulation was run until an energy consumed threshold of 1000 mW-hr was reached.

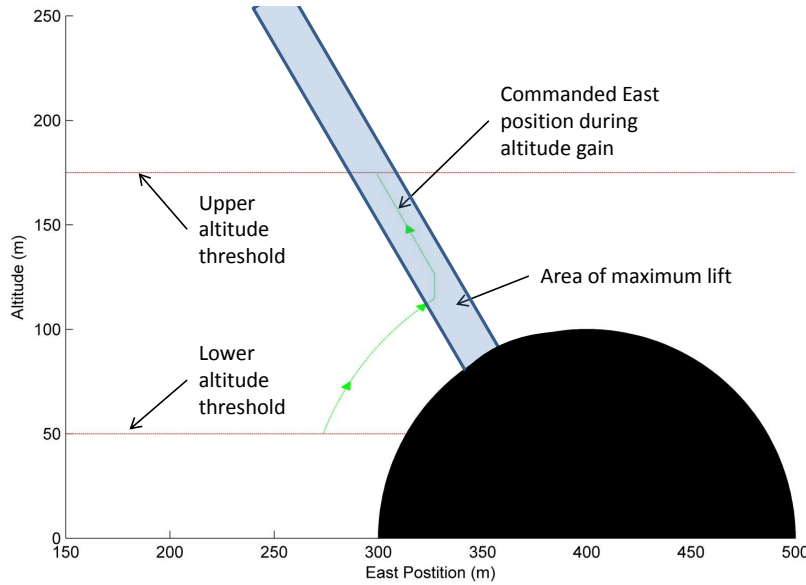


Figure 7. Commanded flight path during altitude gain

If the UAV was able to observe the target without expending any motor energy, the simulation was terminated after several observation iterations. In these simulations we do not consider the power consumed by onboard electronics, only the motor propelling the aircraft.

As a performance baseline to which we can compare energy harvesting results, we first simulated the performance of the ISR scenario without utilizing energy harvesting from the ridge. Results from these simulations are shown in Figures 8 and 9 for targets located 100 m, 400 m, and 700 m from the ridge. Figure 8 shows the flight path followed by the UAV for each of the three target locations from the take-off point to the constant-altitude (100 m) orbit over the target. Figure 9 shows the simulation data for each of the target locations. In each case, the seeability starts off at zero, due to the viewing angle and range, and climbs to a steady value above 0.75 as the UAV orbits the target. For the target 100 m from the ridge, the UAV is able to extract energy from the updraft even though no specific energy harvesting strategy is being utilized. This allows the mission to continue for nearly 1500 seconds before reaching the 1000 mW-hr energy limit. For the targets located 400 m and 700 m from the ridge, there was not a vertical wind component to be exploited. Because the wind fields for these two target scenarios are so similar, the seeability, energy, and power results are nearly identical. In both cases, battery power is required to sustain flight and the UAVs reach the 1000 mW-hr energy threshold after just over 250 seconds of flight.

Figure 10 shows the flight path of a UAV utilizing the ridge lift energy harvesting method presented above. With the target only 100 m from the base of the ridge, the UAV was able to maintain altitude without expending any battery power by surfing back and forth directly over the target. This is confirmed by Figure 11 that shows the UAV power consumption is zero once the UAV reaches the ridge. The seeability metric oscillates between 0.5 and 0.8 as the UAV surfs back and forth over the target along the ridge. The oscillations are due to the changing viewing angle. Using this approach, the UAV was able to observe the target indefinitely without exhausting its battery power.

Figure 12 illustrates the flight path of the UAV observing a target 400 m away from the ridge while harvesting energy from the ridge lift. The path first leads from the take-off point to the target. Immediately after reaching the target, the UAV flies downwind to the ridge where it is able to utilize the updraft to gain altitude. It surfs the ridge until it reaches the 175 m altitude ceiling after which it begins an unpowered glide to the target. Once over the target, the UAV orbits unpowered until it breaks out of the orbit with sufficient altitude to glide to the ridge without dropping below 50 m in altitude, thus preventing the altitude controller from firing the motor to stay above 50 m. Since no energy is used during this observation cycle, the UAV can fly this cycle indefinitely.

Figure 13 shows the effect of the energy harvesting on the instantaneous seeability. The initial spike in seeability occurs as the UAV flies directly over the target at an altitude of 50 m ($t \approx 90$ s). Seeability stays

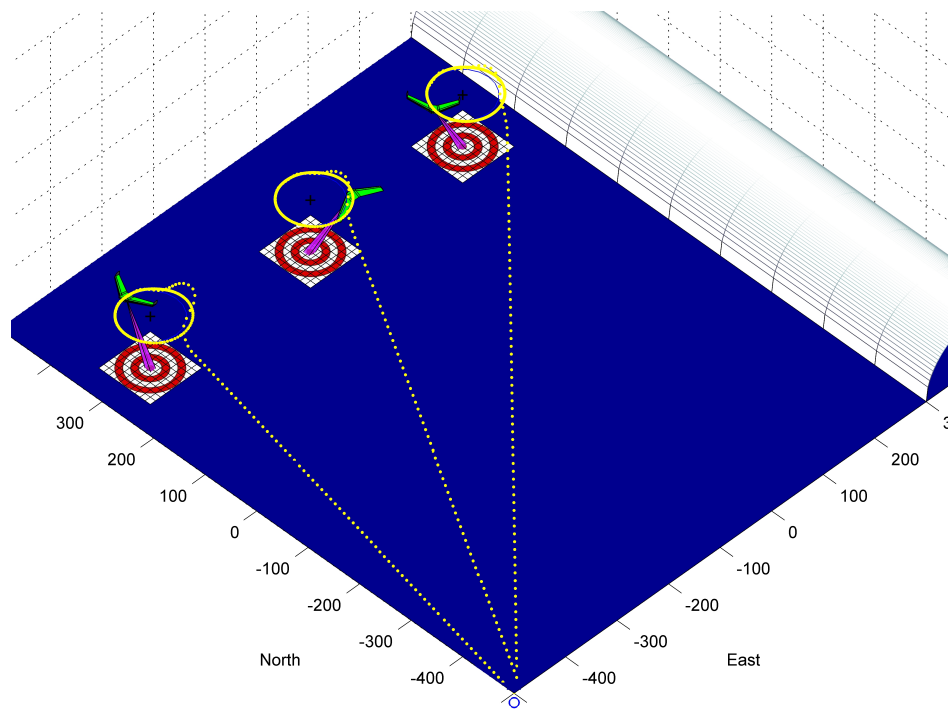


Figure 8. Baseline trajectories for targets 100 m, 400 m, and 700 m from ridge

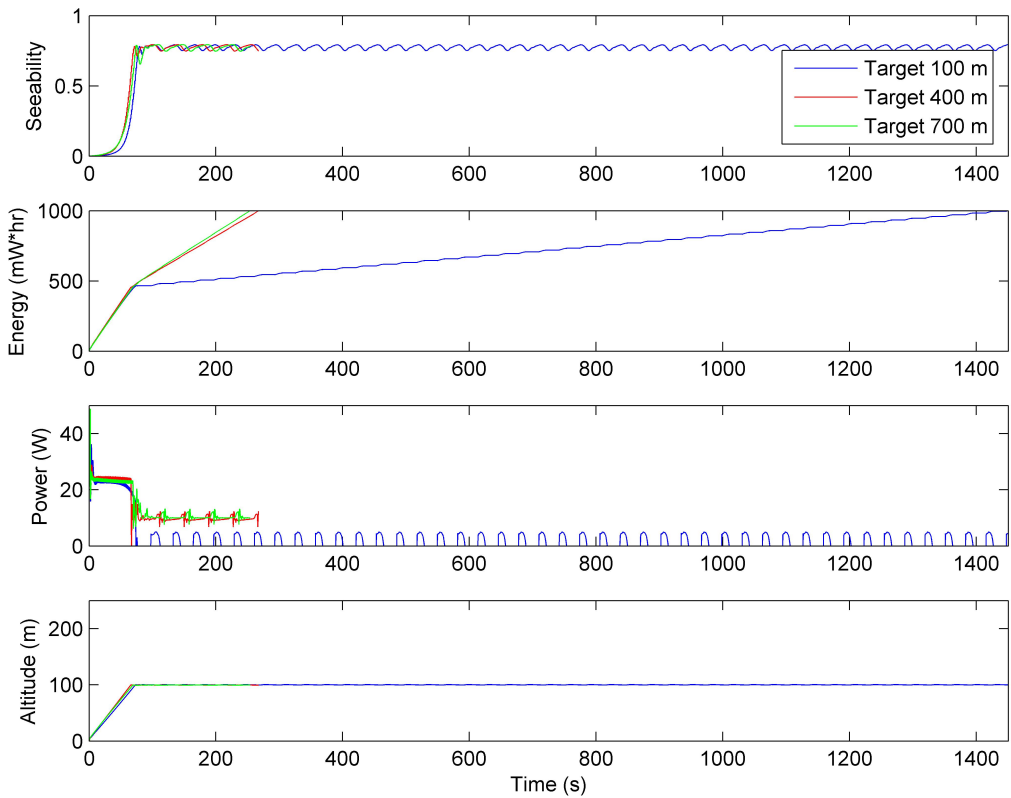


Figure 9. Baseline ISR data for targets 100 m, 400 m, and 700 m from ridge

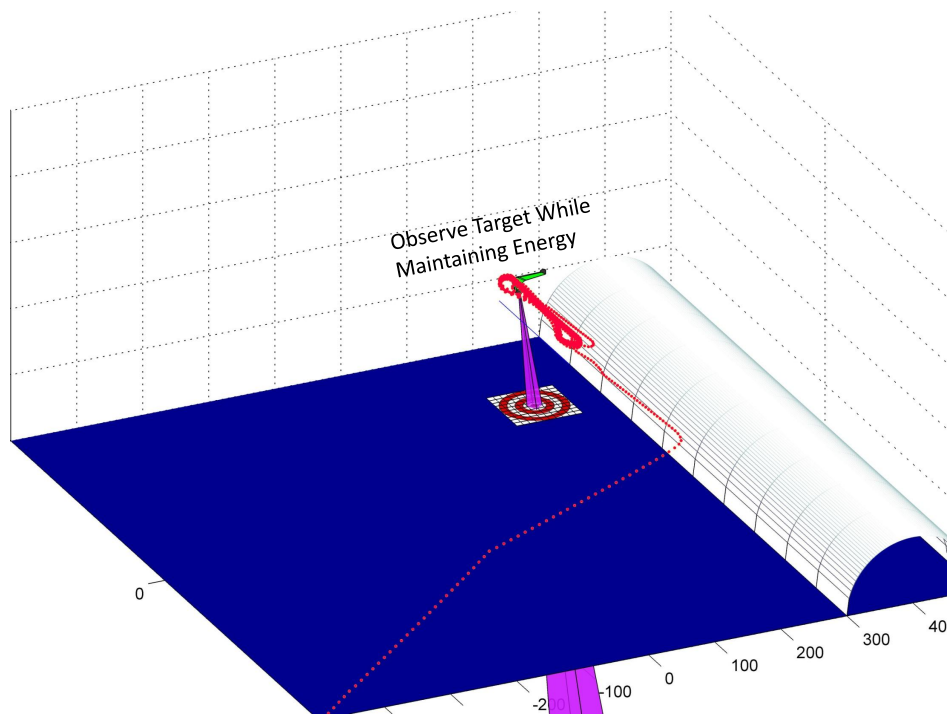


Figure 10. Ridge lift exploiting observation trajectory for target 100 m from ridge

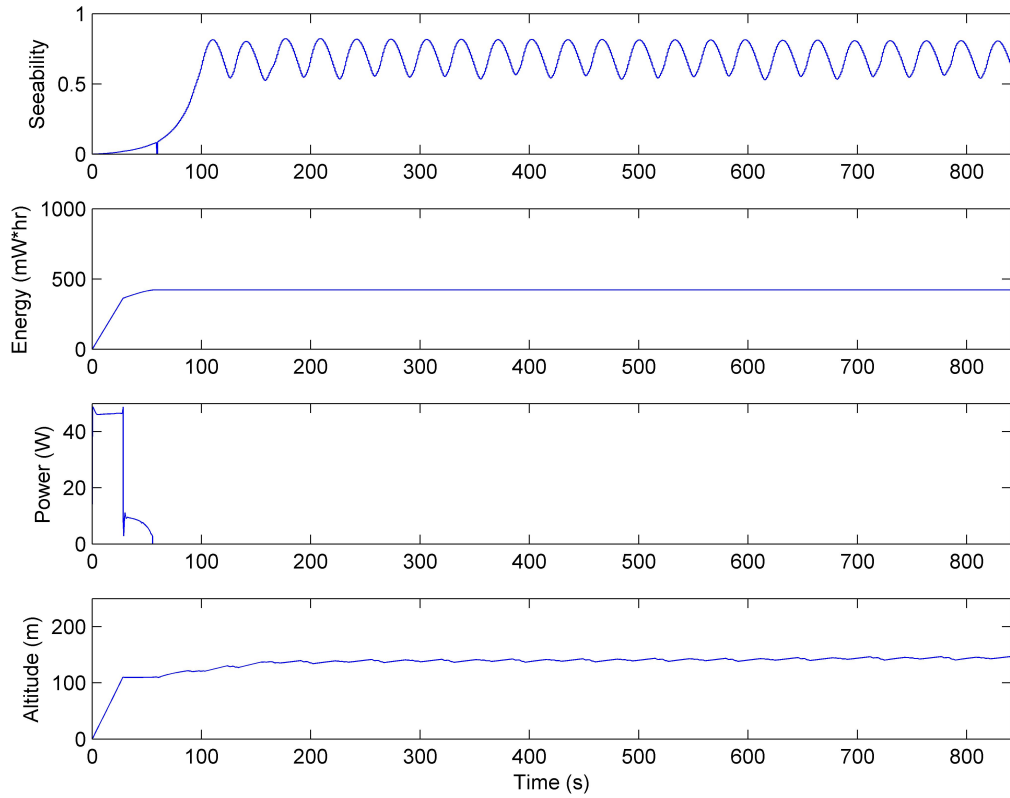


Figure 11. Ridge lift exploiting ISR data for target 100 m from ridge

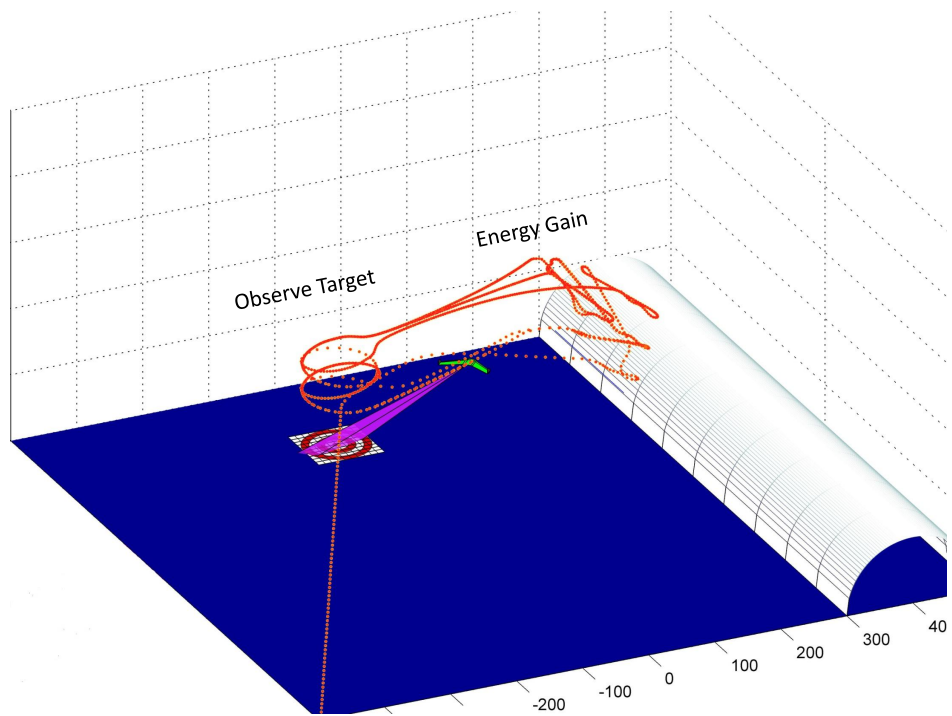


Figure 12. Ridge lift exploiting observation trajectory for target 400 m from ridge

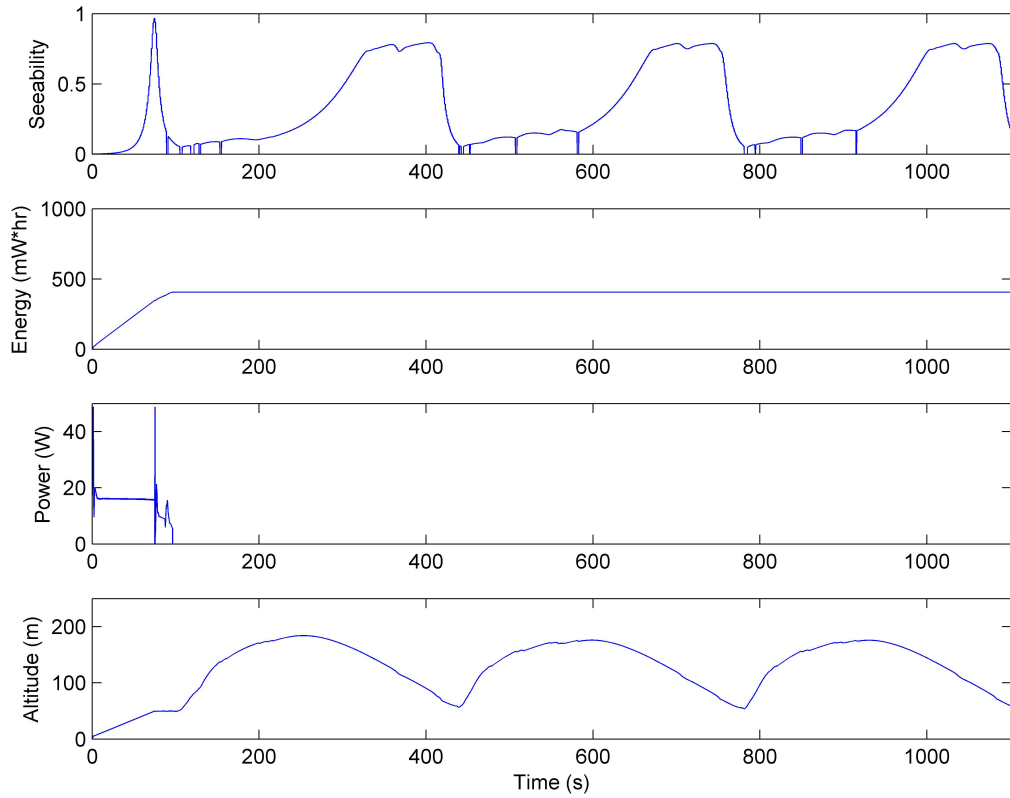


Figure 13. Ridge lift exploiting ISR data for target 400 m from ridge

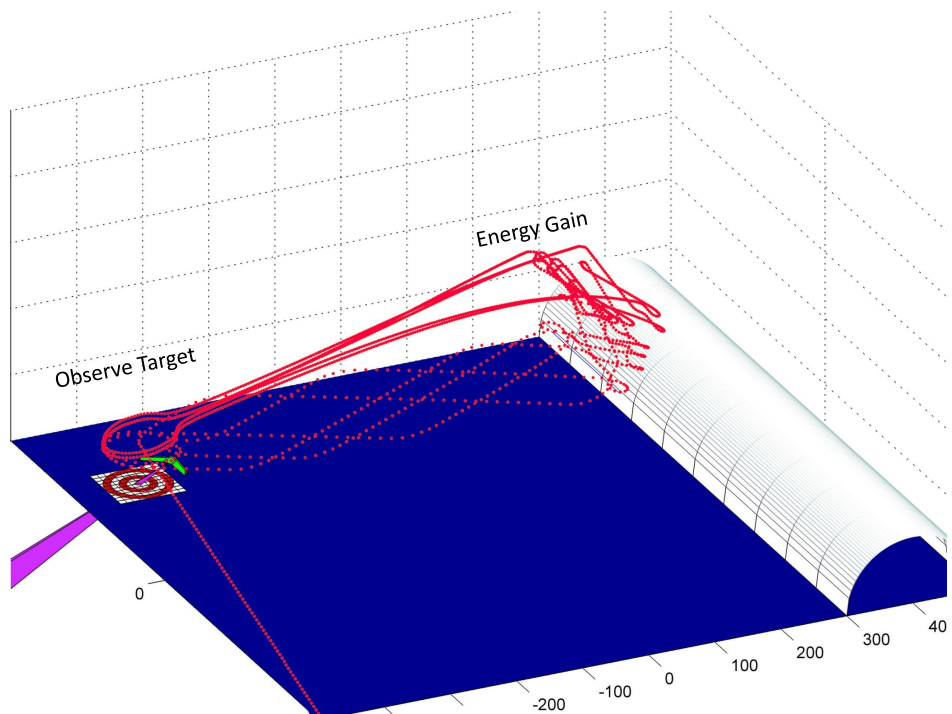


Figure 14. Ridge lift exploiting observation trajectory for target 700 m from ridge

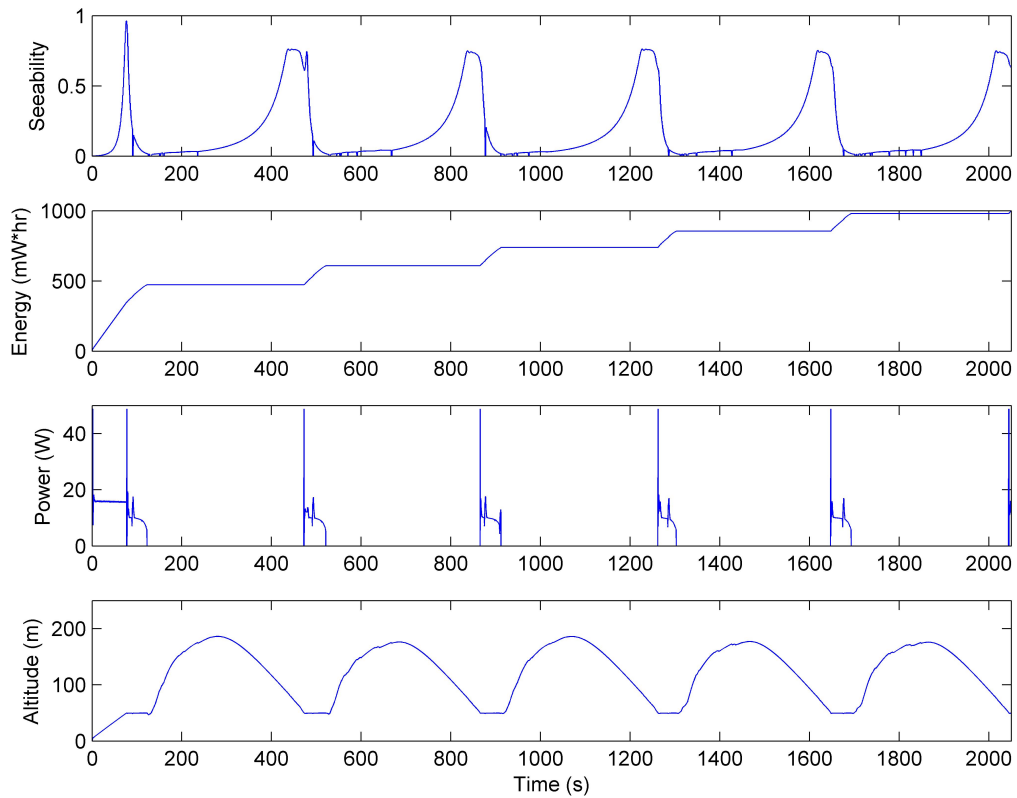


Figure 15. Ridge lift exploiting ISR data for target 700 m from ridge

near a value of 0.1 as the UAV flies toward the ridge and then along the ridge gaining altitude ($t \approx 100$ to 220 s). Seeability increases to about 0.75 as the UAV glides unpowered to the target ($t \approx 220$ to 320 s) and then holds fairly constant while the UAV glides in a descending orbit over the target ($t \approx 320$ to 420 s). At this point, the UAV glides unpowered back to the ridge at the 50 m lower altitude threshold ($t \approx 420$ to 440 s) where the seeability drops off as expected. Notice that once the UAV reaches the ridge initially, no power is expended to sustain flight from this point forward. More energy (in the form of altitude gained) is harvested from the ridge than is expended flying from the target to the ridge and back. This excess energy can then be used to orbit over the target. Although there are gaps where the seeability falls below desired levels, the extended duration over which observations can occur is of significant value.

The third scenario considered has the target at 700 m from the ridge line or seven times the ridge radius. In this scenario, shown in Figure 14, the UAV flies directly to the target and then flies to the ridge to extract energy as in the previous scenario. The UAV climbs unpowered with the help of ridge lift to the 175 m altitude ceiling and then glides toward the target. By the time it reaches the target and completes half an orbit, the UAV hits the low-altitude threshold of 50 m and powers its motor to fly back to the ridge.

Figure 15 shows the time histories for seeability, energy consumption, power, and altitude for the UAV with the target located 700 m from the ridge. In this scenario, the energy harvested from the ridge is less than the energy expended in transit between the ridge and the target. The altitude lost in transit is more than the altitude gained over the ridge. Because of this, battery energy must be used to power the flight from the target to the ridge. These intermittent pulses of power can be seen during the portions of the flight where the UAV is flying at 50 m altitude. These power pulses cause the energy consumption to step up until the 1000 mW-hr limit is reached at just over 2000 seconds. This energy consumed in transit leaves less energy to be consumed in observing the target. With the target positioned as far as it is from the ridge, a better ISR strategy is to fly directly to the target and then use the battery energy to orbit over the target, as in Figures 8 and 9, which show seeability above 0.5 for approximately 190 continuous seconds. The seeability data for the harvesting approach shown in Figure 15 shows that the seeability is intermittently above 0.5 for about 350 seconds. While the harvesting approach nets a higher level of cumulative seeability, the intervals of high seeability may not occur at times critical to the success of the mission.

V. Conclusions

This paper demonstrates the feasibility of utilizing energy harvesting strategies to enhance ISR mission effectiveness. ISR targets near a ridge producing lift were considered. Simulation results showed that for targets of interest at a distance from the ridge less than four times the ridge height, the target could be imaged in intervals that repeat indefinitely provided the wind conditions persist.

VI. Acknowledgments

This research was supported by the Office of Naval Research under STTR contract N00014-09-M-0308 to Mosaic ATM, Inc. and Brigham Young University.

References

- ¹Morse, B., Engh, C., and Goodrich, M., "Aerial Video Coverage Quality Maps and Prioritized Indexing," *International Conference on Human-Robot Interaction*, 2010, Accepted.
- ²Niefeldt, P., Beard, R., Morse, B., and Pledgie, S., "Integrated Sensor Guidance Using Probability of Target Identification," *Proceedings of the American Control Conference*, 2010, Accepted.
- ³Wharington, J. M., "Heuristic Control of Dynamic Soaring," *5th Asian Control Conference*, 2004.
- ⁴Allen, M. J., "Autonomous Soaring for Improved Endurance of a Small Uninhabited Air Vehicle," *AIAA Aerospace Sciences Meeting and Exhibit*, 2005, AIAA-2005-1025.
- ⁵Allen, M. J. and Lin, V., "Guidance and Control of an Autonomous Soaring Vehicle with Flight Test Results," *AIAA Aerospace Sciences Meeting and Exhibit*, 2007, AIAA 2007-867.
- ⁶Edwards, D. J., "Implementation Details and Flight Test Results of an Autonomous Soaring Controller," *AIAA Guidance, Navigation, and Control Conference*, 2008, AIAA 2008-7244.
- ⁷Langelaan, J. W., "Long Distance/Duration Trajectory Optimization for Small UAVs," *AIAA Guidance, Navigation and Control Conference*, August 2007, AIAA 2007-6737.
- ⁸"U.S. Military Specification MIL-F-8785C," November 1980.
- ⁹Griffiths, S. R., "Vector Field Approach for Curved Path Following for Miniature Aerial Vehicles," *AIAA Guidance,*

Navigation, and Control Conference and Exhibit, August 2006, AIAA 2006-6467.

¹⁰Nelson, D. R., Barber, D. B., McLain, T. W., and Beard, R. W., "Vector Field Path Following for Miniature Air Vehicles," *IEEE Transactions on Robotics*, Vol. 37, No. 3, June 2007, pp. 519–529.